Direct Measurement of the Transmission Matrix of a Mesoscopic Conductor

K. L. Shepard, M. L. Roukes, and B. P. Van der Gaag
Bellcore, Red Bank, New Jersey 07701
(Received 31 December 1991)

We have developed an experimental approach which permits evaluation of the entire transmission matrix of a mesoscopic conductor. Results are presented from two new investigations enabled by this technique: (a) We study ballistic multiprobe conductors in the limit of *weak* probe coupling, and (b) we image *modal features* in the distribution function of electrons emerging from a quantum point contact.

PACS numbers: 72.10.Bg, 73.50.Jt

In the mesoscopic regime, electrical conduction involves only a few scatterers and simplifies to become an archetypal quantum mechanical scattering problem [1]. Current incident upon a scatterer can be viewed as a superposition of partial waves. These evolve into outgoing waves according to a matrix of transmission coefficients, **T**, determined by the scattering potential itself.

Transport experiments on microstructures are typically executed in a *multiprobe* configuration. For these, Büttiker [2] has provided a formal link between the quantum transmission picture [1] and measurable, macroscopic resistances. In his model electron *reservoirs*, having chemical potentials μ_i, separately feed the eigenstates of quasi-one-dimensional (1D) *leads*. These leads converge and are coupled at a "junction" region whose scattering matrix subsumes the entire physics of the conductor. The elements of **T**, the transmission coefficients T_{ij}, are fundamental to the theory; from them complicated expressions for the sample's resistance are derived. In experiments, however, *resistances* are most directly obtained but provide little insight into the properties of **T**. Our study is motivated by the desire for a more direct approach.

A multiprobe ballistic conductor, such as illustrated in Fig. 1, constitutes a simple, almost literal realization of Büttiker's model. Wide two-dimensional (2D) regions form reservoirs which connect to short, narrow leads. In these leads current is carried essentially without scattering by electrons occupying only the lowest few transverse modes. The "scatterer" is the electrostatic potential in the locale of the junction region where the leads converge. Its *geometric profile* determines how incoming electrons are ultimately converted to outgoing flux in other leads.

Büttiker's model describes the linear response of a multiprobe conductor as

$$\frac{h}{2e} I_i = -N_i \mu_i + \sum_j T_{ij} \mu_j , \qquad (1)$$

where i and j are indices labeling the leads. In steady state, chemical potentials μ_j (and, thus, voltages, $V_j = \mu_j/e$) develop at the reservoirs in response to the imposed currents I_i [3]. The transmission coefficient T_{ij} represents the *total* probability of transmission from lead $j \rightarrow i$ for states at the Fermi energy, and is given by a sum over all occupied modes (indices k,l) in both leads: $T_{ij} = \sum_{kl} |t_{ij,kl}|^2$. N_i is the number of propagating modes; $N_i = \sum_j T_{ij}$. Unlike the transmission probabilities, $|t_{ij,kl}|^2$, the coefficients T_{ij} can exceed unity: $T_{ij} \in [0, N_i]$. By external connections, reservoirs are generally forced to serve as either current (I) or voltage (V) "contacts." In conjunction with Eq. (1), this yields complicated four-probe resistances of general form $R_{kl,mn} = h(T_{mk}T_{nl} - T_{ml}T_{nk})/2e^2 D$, where D is any cofactor of the matrix defined by Eq. (1) [2]. Here, indices reflect current flow from reservoirs $k \rightarrow l$, yielding a potential drop from m to n.

Viewed from the perspective of Eq. (1), conventional resistance measurements implicitly involve the imposition of boundary conditions upon the *currents* I_i. If, instead, we fix the *chemical potentials*, Eq. (1) is immediately simplified. Specifically, if we source a current I_1 into reservoir 1 while *equalizing* μ_i at the other reservoirs by an ideal short-circuit connection, $\mu_2 = \mu_3 = \mu_4 \equiv 0$, Eq. (1)

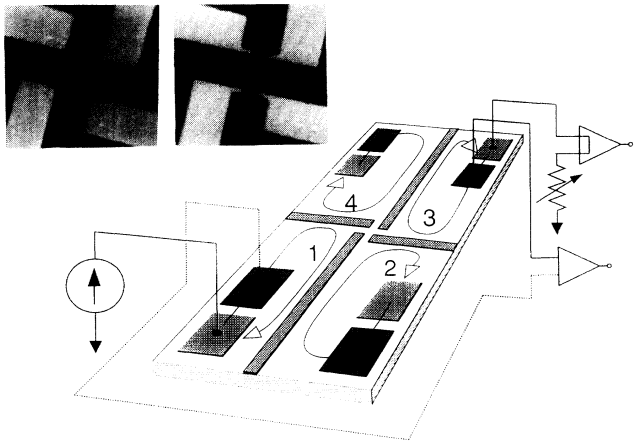

FIG. 1. Configuration for the **T**-measurement technique. Four long gate electrodes at the surface of a 2DEG heterojunction (*light shading*) electrostatically isolate four rectangular 2D reservoirs. From these, narrower channels lead to a central junction region. Arrows show the direction of current flow for B directed upward. Assignment of current (light shading) and voltage (dark shading) contacts depends upon field orientation. For clarity, external connections are shown only for reservoirs 1 and 3. *Left (right) insets*: Electron micrograph of *open (pinched)* junction regions. Gates separated by 400 nm define the leads. Weak coupling is obtained in *pinched* cross junctions by 150-nm-wide constrictions formed between two 50-nm-wide gate fingers.

then reduces to $(h/2e)(I_1\ I_2\ I_3\ I_4) = -N_1(\mu_1\ 0\ 0\ 0) + (\mu_1\ 0\ 0\ 0)\mathbf{T}$. Under these conditions the off-diagonal T_{ij} become directly proportional to the currents, $T_{i1} = (h/2e)I_i/\mu_1$, while $T_{11} - N_1 = (h/2e)I_1/\mu_1$. Other columns of $\mathbf{T}$ ($i \neq 1$) are obtained by changing the source lead and following the same procedure.

Practically, of course, real short circuits between the reservoirs will have finite resistance. The resulting path-specific potential drops render external short circuits ineffective at equalizing the μ_i which are internal to the sample. We circumvent this difficulty by including a separate I contact and V contact at each reservoir [4], and by introducing external, variable terminating impedances between each (sink) I contact and "ground" (Fig. 1). This enables us to simultaneously monitor *all* the μ_i in the presence of current flow and null differences between them by iterative adjustment of the terminating impedances [5,6]. In experiments, we study the evolution of $\mathbf{T}$ in response to swept external "fields" (e.g., magnetic field, gate bias, temperature). In this situation the μ_i must be equalized dynamically [7]. In practice we find self-consistent adjustment of terminating impedances less convenient than an alternate procedure employing static terminations. This involves building a set of linear equations through successive measurements (sweeps) which we ultimately solve to obtain $\mathbf{T}$ [6].

The experiments are carried out using *four-probe* samples specifically designed for these measurements [6]; these require eight contacts (Fig. 1). Measurements reported here are carried out at ~ 2 K using a 10-nA drive current. Our approach provides a set of transmission coefficients satisfying the reciprocity relation [2], $T_{ij}(B) = T_{ji}(-B)$, to within the accuracy of the measurements (typically a few percent). Also, we verify that "reconstituted" resistances, formed using *measured* T_{ij} in expressions for $R_{kl,mn}$ from Eq. (1), are consistent with direct resistance measurements [Figs. 2(c),2(e)].

We first apply this technique to compare transport in the complementary limits of *weak* and *strong* probe coupling. The "open" cross junction (Fig. 1, left inset) exemplifies strong coupling; at the junction no geometrical distinction exists between "voltage" and "current" probes. The opposite limit requires voltage probes decoupled from the main current path, i.e., accepting infinitesimal transmission t compared to that along the main conductor, T [8]. This limit, $t/T \ll 1$, is envisioned as enabling noninvasive measurement of the local chemical potential and, thereby, the intrinsic transport properties of quasi-1D wires [8–10]. We achieve weak coupling in "pinched" cross junctions (Fig. 1), utilizing quantum point contacts (QPC's) to separate probes from the main conductor.

We summarize our studies by a representative set of results from a *pinched* cross junction in Fig. 2. In panels (a)–(e), we display measurements obtained at three gate voltages (labeled *a,b,c*). At these biases transmission through the QPC's is small, $t \sim 0.5$, 1.5, and 2.5, respectively [Fig. 2(e), inset], while transmission along the main conductor is larger, $T \sim 7$, 8, and 10. Bias *a* provides the weakest coupling: $t/T \sim 0.07$.

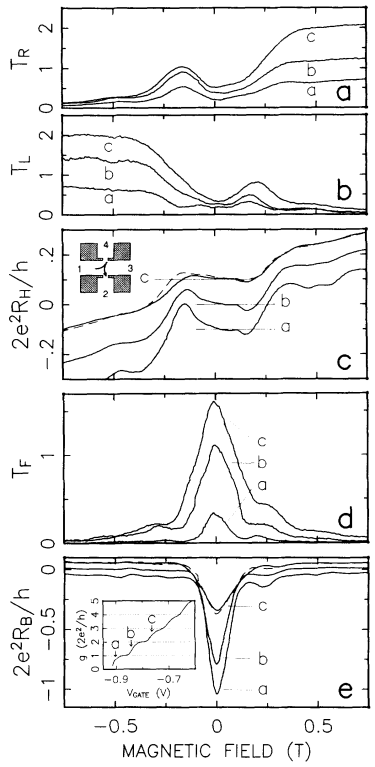

FIG. 2. Data from a *pinched* cross junction at three gate voltages labeled *a*, *b*, and *c*, at which $V_G \sim -0.90$, -0.84, and -0.76 V, respectively. The corresponding quantized conductance through the constrictions, as shown in panel (e) (inset), indicate transmission of ~ 0.5, 1.5, and 2.5, respectively. (a),(b) "Turning coefficients," T_R and T_L, into the right and left probes. Because of the device symmetry, $T_R = T_{21}(B) \sim T_{43}(B)$ and $T_L = T_{41}(B) \sim T_{23}(B)$. (c) Hall resistance, $R_H = R_{13,24}(B)$, reconstituted from measured T_{ij} (solid curves). Also shown is R_H measured conventionally at bias, *c* (dashed). Curves for *a* and *c* are offset by $+0.1$ and -0.1, respectively. Inset: A trajectory causing a peak in T_R at negative B. (d) Forward transmission coefficient, $T_F = T_{42}(B)$, for electrons propagating through both constrictions as depicted in Fig. 3 (inset). (e) Bend resistance, $R_B = R_{12,43}(B)$ reconstituted from measured T_{ij}. Also shown is R_B directly measured at bias *c* (dashed). Curves for *a* and *c* are offset by 0.05 and -0.05, respectively.

We first discuss the "turning coefficients," T_R and T_L, for electrons injected into a *pinched* cross junction and collected into weakly coupled right and left leads. With sufficient magnetic field (normal to the 2D plane) the Lorentz force directs most flux into *one* of the side leads [Figs. 2(a) and 2(b)]. However, additional features appear in the other lead at fields where little flux should be collected. Most prominent are the peaks in T_R (and T_L) at $B \approx -0.2$ T ($+0.2$ T). *Open* cross junctions exhibit similar behavior [6]. As a result, the (reconstituted) Hall resistance R_H is first seen to quench [11] then reverse

sign [12] as transmission into the probes is reduced [biases $c \rightarrow a$, Fig. 2(c)]. Note that only for bias c can R_H be directly measured [Fig. 2(c)]; for biases a and b weak coupling precludes resistance measurements, which utilize voltage probes [13].

We ascribe these features to electron flux specularly reflected from the junction boundary into the opposite probe [Fig. 2(c), inset]. Of mechanisms proposed to explain the R_H anomaly in microjunctions [14] only this "rebound" effect, first inferred from resistance measurements [12], appears to be consistent with the structure we observe in T_L and T_R for both *pinched* and *open* cross junctions. Most surprising is that this effect *grows* as the probes become decoupled (Fig. 3, curve c). Presumably, if these phenomena stem from *junction scattering* they should instead vanish in this limit. Calculations using idealized potentials to model weakly coupled probes confirm this expectation [9,10]. However, in our data, these and other signatures of junction scattering persist even in the limit of weak coupling [15]. Because the potentials which can be imposed upon a 2DEG are "soft" (i.e., spatially smoothed), even in this limit the main conductor is evidently perturbed by the proximity of a probe.

Our second application elucidates new details of transport in a QPC. The *pinched* cross junctions (Fig. 1) constitute a collinear pair of QPC's embedded within a four-probe geometry equipped for T_{ij} measurement. Electron beam collimation by a QPC [16] has been demonstrated using a series arrangement of constrictions [17]. Our approach unveils new features when the emitted flux is small. Figure 2(d) shows T_F, the forward transmission coefficient for electrons propagating through both QPC's,

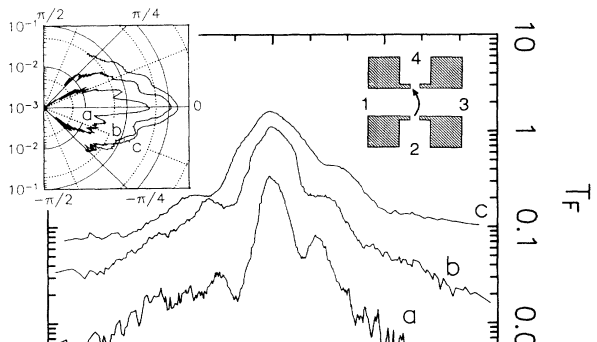

FIG. 3. Angular profile of the "beam" emerging from one constriction at biases a, b, and c. T_F is shown as a function of angle of emission. At these biases the separation between points contacts, d, are ~210, ~220, and ~270 nm, respectively. The corresponding densities n_s within the junction are (~1.8, ~2.0, and ~2.2)×10^{11} cm^{-2}, respectively. *Right inset:* Schematic representation of the semiclassical trajectory determining T_F. *Left inset:* Polar representation of the emerging "beam" for biases, a,b,c, employing a logarithmic radial coordinate.

i.e., from "injector" to "collector." Upon application of finite B, the emerging "beam" is deflected from the collector and, thus, T_F falls. For *open* cross junctions this occurs monotonically, but in *pinched* cross junctions we find a *nonmonotonic* decay. New features emerge, offset from the maximum at $B=0$. However, little or no corresponding structure is resolved in the bend resistance [18] R_B when obtained by direct four-probe measurement [Fig. 2(e), trace c], as utilized in Ref. [17].

The B dependence of T_F allows a sensitive momentum spectroscopy. We deduce the angular profile of the injected beam assuming classical propagation between the QPC's [17], and approximation valid at $T \sim 2$ K where significant phase averaging occurs. Assuming *point* collection, electrons emitted at angle θ are collected when $r_c \sin\theta = d/2$. Here $r_c = (h/eB)(n_s/2\pi)^{1/2}$ is the cyclotron radius and d is the distance between constrictions. We obtain n_s from the quantum Hall effect, where d is extracted from the quantized conductance along the main channel. Figure 3 shows the profile of the collected beam, $T_F(\theta)$ [19].

Although propagation within the junction is essentially classical in these experiments, transport at the QPC's is *not*. We constrict them to the point where, at most, only a few modes propagate. In this quantum regime side lobes appear in the emerging beam (Fig. 3, inset). This structure cannot be attributed to diffraction; calculated secondary diffraction maxima are several orders of magnitude smaller in intensity than the central beam [6]. Features of this magnitude can result from injection of a *multimode* distribution into a semi-infinite 2D region. Especially striking, however, is that the data show side lobes even for bias a, i.e., *even when only the lowest transverse mode propagates through the constriction.* This clearly implies that intermode scattering generates higher modal components in the outgoing beam. Our calculations, described below, support this and indicate that conductance may remain approximately quantized [20] (as is exhibited in our experiments).

Although electrodes inducing a QPC may be morphologically smooth, the actual potential imposed upon the electrons will not be. Calculations indicate that ionized donors induce strong potential fluctuations [21]. We believe that close to pinch-off this, *in general*, results in transport controlled by a single narrow region, i.e., a *critical path* [Fig. 4(a), left inset]. We illustrate this by recursive Green's-function calculations [22] employing a model potential [Fig. 4(a)]. Its narrowest (I) and transition (III) regions are connected by a short zone (II) where the channel widens abruptly and the potential becomes spatially *nonadiabatic*, i.e., $dW/dx > 1/N(x)$, where $N(x) \sim k_F W(x)/\pi$ and $W(x)$ is the (transverse) width at (longitudinal) position x [23]. Our calculations yield $T(\theta)$, the angular profile of the emerging beam (Fig. 4). Modal features are exhibited, at $\Theta_{\pm}^{(n)} \sim \pm \sin^{-1}(n\pi/k_F W_{III})$, similar to those observed experimentally. The transition region (III) not only determines

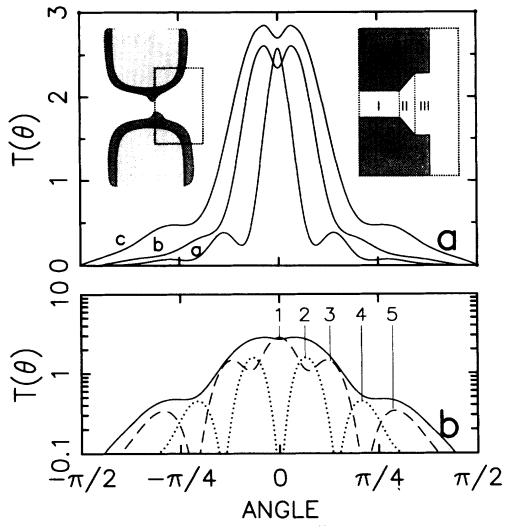

FIG. 4. Calculated angular profile of the momentum distribution emerging from a constriction. Curves *a*, *b*, and *c* correspond to 1, 2, and 3 injected modes, respectively. (a) $T(\theta)$, flux per unit angle normalized by $\hbar k_F/m^*$. *Left inset*: Critical path model of a quantum point contact. The depletion region defining the *effective* boundaries of the constriction (dark shading) do not follow the smooth contours of the gates themselves (light shading). *Right inset*: Model potential for the half of the constriction contained within the dashed box of the left inset. The narrowest region (I) of width W_I and potential V_I empties into the transition region (III) of fixed width $W_{III}=3.2\lambda_F$, length $L=1.6\lambda_F$, and potential $V_{III}=0$. These are connected by a nonadiabatic region (II), of fixed length, $1.6\lambda_F$, with width and potential *both* linearly graded to match at regions I and III. For curves *a*, *b*, and *c*, $W_I=(0.95, 1.3,$ and $1.6)\lambda_F$, respectively; while $V_I=(0.38, 0.04,$ and $0.00)E_F$, respectively. (b) Modal decomposition of curve *c* into even (dotted) and odd (dashed) parity components. These are separately conserved because of the mirror-plane symmetry of the potential. Calculated angular positions for transverse modes 1 through 5 of region III are labeled. For curve *c* of panel (a), the predominant "shoulders" of the sum curve (solid) arise from intermode scattering into the fourth and fifth modes. For curve *a* of panel (a), however, we find that analogous shoulders arise *solely* due to scattering from mode $1\rightarrow 3$.

the angular position of these features, but also their angular spread. We find that region III must be of length $L\geq\lambda_F$ for side lobes to emerge. For $L<\lambda_F$, diffraction broadens the modal components into a single peak [6,24].

Our observations show that conductance through a QPC can remain approximately quantized even in the presence of intermode scattering. This is consistent with a picture where conductance is controlled by a critical path which induces transitions in the emerging beam while causing minimal backscattering.

We thank A. Scherer for assistance. M.L.R. acknowledges helpful discussions with M. Büttiker during initial phases of this work (1988). K.L.S. gratefully acknowledges support from the Hertz Foundation and the NSF through Grant No. EID 87-11693.

[1] R. Landauer, Philos. Mag. **21**, 863 (1970).
[2] M. Büttiker, Phys. Rev. Lett. **57**, 1761 (1986).
[3] Here, positive currents imply flow *into* the reservoirs.
[4] Correct assignment minimizes contributions to the V_j from the Hall potential. For the two-probe case, see H. van Houten *et al.*, Phys. Rev. B **37**, 8534 (1988).
[5] Small *internal* voltage drops occur due to the geometrical "spreading" resistance between each reservoir and lead. These can be measured, but cannot be nulled. Our sample design reduces these to become few percent corrections to the (quantized) conductance of the (few-mode) leads themselves. At finite temperature, the T_{ij} actually obtained are *energy-averaged* coefficients: $\int T_{ij}(E)\times(-\partial f/\partial E)dE$ (Ref. [6]).
[6] K. Shepard, M. L. Roukes, and B. P. Van der Gaag (unpublished); M. L. Roukes, K. Shepard, and B. P. Van der Gaag, in *Science and Technology of Mesoscopic Structures*, edited by S. Namba *et al.* (Springer, Tokyo, 1992).
[7] Potential drops along connections to external "ground" vary with external fields. This precludes any static method of inferring T_{ij} based solely upon current measurements; [cf. S. K. Greene *et al.*, J. Phys. Condens. Matter **3**, 1961 (1991)].
[8] H.-L. Engquist and P. W. Anderson, Phys. Rev. B **24**, 1151 (1981).
[9] F. M. Peeters, Phys. Rev. Lett. **61**, 589 (1988).
[10] H. Akera and T. Ando, Phys. Rev. B **39**, 5508 (1989).
[11] M. L. Roukes *et al.*, Phys. Rev. Lett. **59**, 3011 (1987).
[12] C. J. B. Ford *et al.*, Phys. Rev. Lett. **62**, 2723 (1989).
[13] In conventional four-probe measurements, the steady-state μ_i attained by any *voltage* reservoir fed by a weakly coupled probe is, in general, rendered meaningless by parasitic leakage currents and finite voltmeter input impedance.
[14] For a recent review, see H. U. Baranger *et al.*, Phys. Rev. B **44**, 10637 (1991).
[15] Even with almost completely constricted side probes, certain trajectories *backscatter* strongly from slight distortions of the main channel within a specific field range (Ref. [6]).
[16] C. W. J. Beenakker and H. van Houten, Phys. Rev. B **39**, 10445 (1989).
[17] C. W. Molenkamp *et al.*, Phys. Rev. B **41**, 1274 (1990).
[18] Y. Takagaki *et al.*, Solid State Commun. **68**, 1051 (1988); G. Timp *et al.*, Phys. Rev. Lett. **60**, 2081 (1988).
[19] For ballistic propagation, $T_F(\theta)\propto\min[T_i(\theta),T_c(\theta)]$, where subscript i (c) represents injector (collector). The proportionality factor involves the effective solid angle subtended by the collector (Ref. [6]).
[20] E. Castano and G. Kirczenow, Phys. Rev. B **45**, 1514 (1992).
[21] J. A. Nixon and J. H. Davies, Phys. Rev. B **41**, 7929 (1990).
[22] See, e.g., Ref. [14], or K. Shepard, Phys. Rev. B **44**, 9088 (1991), and references therein.
[23] A. Yacoby and Y. Imry, Phys. Rev. B **41**, 5341 (1990).
[24] D. van der Marel and E. G. Haanappel, Phys. Rev. B **39**, 7811 (1989).

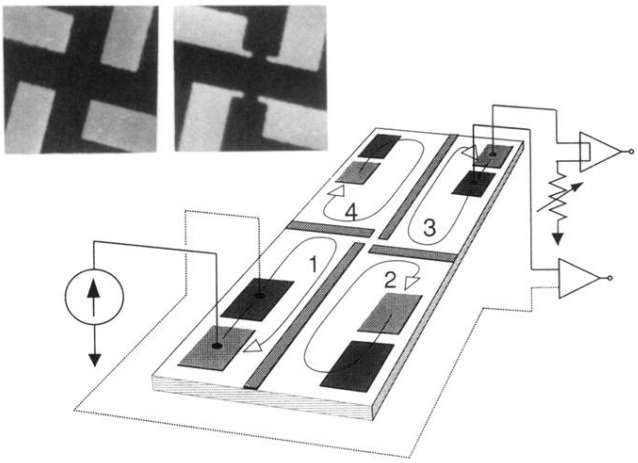

FIG. 1. Configuration for the **T**-measurement technique. Four long gate electrodes at the surface of a 2DEG heterojunction (*light shading*) electrostatically isolate four rectangular 2D reservoirs. From these, narrower channels lead to a central junction region. Arrows show the direction of current flow for B directed upward. Assignment of current (light shading) and voltage (dark shading) contacts depends upon field orientation. For clarity, external connections are shown only for reservoirs 1 and 3. *Left (right) insets*: Electron micrograph of *open (pinched)* junction regions. Gates separated by 400 nm define the leads. Weak coupling is obtained in *pinched* cross junctions by 150-nm-wide constrictions formed between two 50-nm-wide gate fingers.

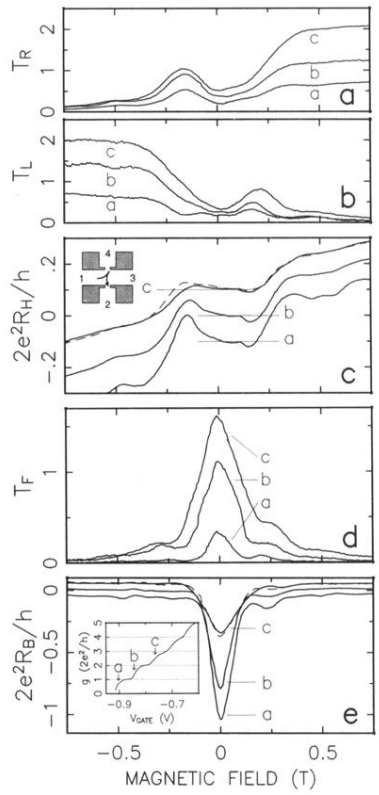

FIG. 2. Data from a *pinched* cross junction at three gate voltages labeled *a*, *b*, and *c*, at which $V_G \sim -0.90$, -0.84, and -0.76 V, respectively. The corresponding quantized conductance through the constrictions, as shown in panel (e) (inset), indicate transmission of ~ 0.5, 1.5, and 2.5, respectively. (a),(b) "Turning coefficients," T_R and T_L, into the right and left probes. Because of the device symmetry, $T_R = T_{21}(B) \sim T_{43}(B)$ and $T_L = T_{41}(B) \sim T_{23}(B)$. (c) Hall resistance, $R_H = R_{13,24}(B)$, reconstituted from measured T_{ij} (solid curves). Also shown is R_H measured conventionally at bias, *c* (dashed). Curves for *a* and *c* are offset by $+0.1$ and -0.1, respectively. Inset: A trajectory causing a peak in T_R at negative *B*. (d) Forward transmission coefficient, $T_F = T_{42}(B)$, for electrons propagating through both constrictions as depicted in Fig. 3 (inset). (e) Bend resistance, $R_B = R_{12,43}(B)$ reconstituted from measured T_{ij}. Also shown is R_B directly measured at bias *c* (dashed). Curves for *a* and *c* are offset by 0.05 and -0.05, respectively.

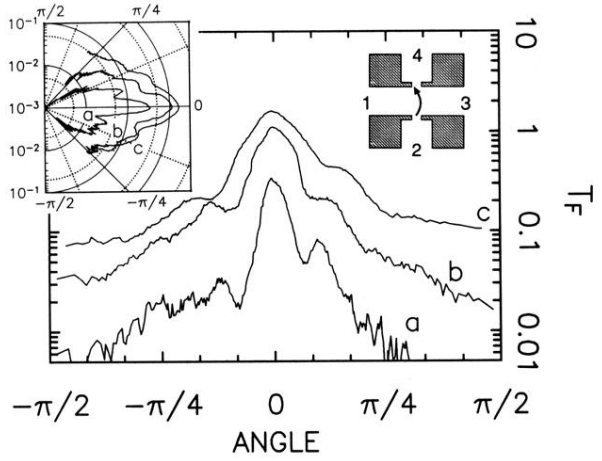

FIG. 3. Angular profile of the "beam" emerging from one constriction at biases *a*, *b*, and *c*. T_F is shown as a function of angle of emission. At these biases the separation between points contacts, *d*, are ~210, ~220, and ~270 nm, respectively. The corresponding densities n_s within the junction are $(\sim 1.8, \sim 2.0, \text{ and } \sim 2.2)\times 10^{11}$ cm^{-2}, respectively. *Right inset:* Schematic representation of the semiclassical trajectory determining T_F. *Left inset*: Polar representation of the emerging "beam" for biases, *a*,*b*,*c*, employing a logarithmic radial coordinate.

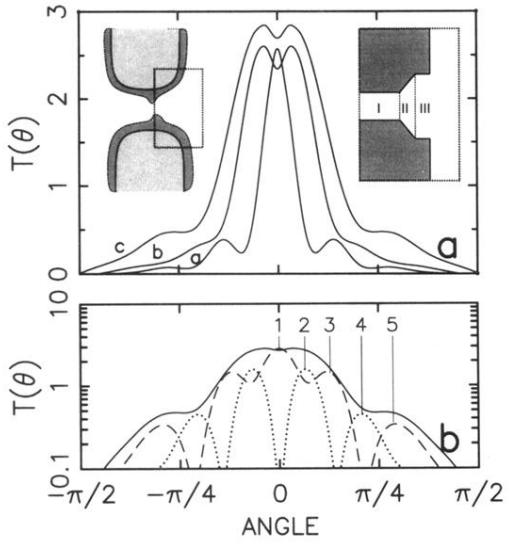

FIG. 4. Calculated angular profile of the momentum distribution emerging from a constriction. Curves *a*, *b*, and *c* correspond to 1, 2, and 3 injected modes, respectively. (a) $T(\theta)$, flux per unit angle normalized by $\hbar k_F/m^*$. *Left inset*: Critical path model of a quantum point contact. The depletion region defining the *effective* boundaries of the constriction (dark shading) do not follow the smooth contours of the gates themselves (light shading). *Right inset*: Model potential for the half of the constriction contained within the dashed box of the left inset. The narrowest region (I) of width W_I and potential V_I empties into the transition region (III) of fixed width $W_{III}=3.2\lambda_F$, length $L=1.6\lambda_F$, and potential $V_{III}=0$. These are connected by a nonadiabatic region (II), of fixed length, $1.6\lambda_F$, with width and potential *both* linearly graded to match at regions I and III. For curves *a*, *b*, and *c*, $W_I=(0.95, 1.3,$ and $1.6)\lambda_F$, respectively; while $V_I=(0.38, 0.04,$ and $0.00)E_F$, respectively. (b) Modal decomposition of curve *c* into even (dotted) and odd (dashed) parity components. These are separately conserved because of the mirror-plane symmetry of the potential. Calculated angular positions for transverse modes 1 through 5 of region III are labeled. For curve *c* of panel (a), the predominant "shoulders" of the sum curve (solid) arise from intermode scattering into the fourth and fifth modes. For curve *a* of panel (a), however, we find that analogous shoulders arise *solely* due to scattering from mode $1 \rightarrow 3$.